Available online at www.sciencedirect.com
SCIENCE DIRECT®
Journal of Solid State Chemistry 178 (2005) 1414–1421
JOURNAL OF SOLID STATE CHEMISTRY
www.elsevier.com/locate/jssc

Low-temperature synthesis of fine $BaMgAl_{10}O_{17}:Eu^{2+}$ phosphor based on the solubility isotherms

Dong-Kuk Kim[a,*], Sung-Ho Hwang[a], In-Gyu Kim[a], Jung-Chul Park[b], Song-Ho Byeon[c]

[a]*Department of Chemistry, College of Natural Sciences, Kyungpook National University, Daegu 702-701, Korea*
[b]*Department of Nano Materials Science and Engineering, Nano Applied Technology Research Center, Silla University, Busan 617-736, Korea*
[c]*College of Environment and Applied Chemistry, Kyung Hee University, Kyung Ki 449-701, Korea*

Received 25 August 2004; received in revised form 15 November 2004; accepted 21 November 2004
Available online 16 March 2005

Abstract

A homogeneous and stoichiometric $BaMgAl_{10}O_{17}:Eu^{2+}$ (BAM) phosphor powder has been prepared by the citrate route. Solubility isotherms have been calculated for metal–citric acid–water system at 25 °C to predict the optimum pH condition, which was found to be pH = 7 for preparing pure and stable metal citrate complexes. Well crystallized and sub-micrometer-sized BAM particles could be obtained by thermal decomposition of the optimally prepared citrate precursor at a temperature as low as 1150 °C. Though the luminescent properties of the present samples under UV excitation well reflect the bulk properties, VUV excitation has exhibited the luminescent properties greatly influenced by the surface, which might be due to the fine particle. The maximum luminance of the samples heat treated at 1350 °C was 105% in comparison with that of the commercial BAM under VUV excitation.

Keywords: Solubility isotherm; Luminescence; BAM phosphor

1. Introduction

The blue lighting Eu-doped barium magnesium aluminate, $BaMgAl_{10}O_{17}:Eu$ (BAM), has been of great interest because of its high luminescent efficiency under vacuum ultraviolet (VUV) irradiation of the plasma display panels (PDP), which is the most prominent among the recent emissive flat displays [1,2]. In addition, since this material exhibits the blue emission band appropriate for fluorescent lamp as well as high luminescent efficiency and stability under ultraviolet irradiation, it has been used in trichromatic fluorescent lamp [3,4]. However, a very high temperature in a complete reducing atmosphere is needed for the synthesis of this material by conventional solid-state synthesis [5,6], which not only takes up too much expense but also results in the large hexagonal plate-like particles with a high aspect ratio. Considering the short penetration depth of VUV radiation due to a large absorption coefficient in fundamental absorption [7,8], small-sized phosphor particles with large surface area would be more effective for PDP application. Moreover, for effective glass coating, fine particles with spherical morphology are preferred to large plate-like particles. In this respect, we have studied a synthetic route for Eu-doped BAM phosphor material with a fine particle size as well as high crystallinity even at a low temperature.

$BaMgAl_{10}O_{17}$ has the β-alumina type structure (space group = $P6_3/mmc$) and can be derived from sodium β-alumina by replacing $(NaAl)^{4+}$ with $(BaMg)^{4+}$ [6,9]. BAM has been conventionally prepared by the solid-state reaction of corresponding oxides, carbonates, and hydroxides under a reducing atmosphere at temperatures as high as at least 1500 °C for several hours. In order to reduce the reaction temperature and control the

*Corresponding author. Fax: +82 53 950 5331.
E-mail address: kimdk@knu.ac.kr (D.-K. Kim).

0022-4596/$ - see front matter © 2004 Elsevier Inc. All rights reserved.
doi:10.1016/j.jssc.2004.11.022

particle growth, additional fluxes such as metal fluoride (AlF_3 or MgF_2) or boria (B_2O_3) have been also used [10–13]. However, usage of additional fluxes could not exclude the stabilization of undesirable elements such as fluorine or boron into the host material, and also requires that the post-washing processes to get rid of remaining fluxes or soluble impurities. Since the alkaline earth aluminates are refractory compounds (melting point of BAM = 1920 °C), a high firing temperature is necessary for diffusion of rare-earth ions into the crystal lattice and to obtain single-phase oxide phosphors. However, it imposes high cost and energy requirements on the production process. Also, high temperature firing often leads to compositional and structural fluctuations, abnormal grain growth, which is detrimental to phosphor efficiency. Furthermore, the use of phosphor particles with high uniformity in size and morphology is crucial to improve the performances of flat panel displays and lamps.

As alternative techniques, there have been recent reports on hydrolysis of metal alkoxides [14], combustion synthesis [4], hydrothermal process [1], spray pyrolysis [15–17], and microwave irradiation method [1] to prepare BAM powders with spherical shape, fine size, narrow size distribution, and non-aggregation characteristics.

Another attractive route to refractory oxide compounds is a citrate sol–gel method utilizing the strong chemical complex between metal cations and citrates [18]. It has been recognized that the sol–gel process using metal–organic precursors (usually metal citrates in the conventional Pechini process [19]) can lead to fine and homogeneous powders with controlled stoichiometry as also proved in our previous reports [20]. In addition, high-temperature rare-earth diffusion is not necessary with this method owing to intimate atomic-scale mixing of the elements in the precursor solution. In this sol–gel process, it is highly desirable to obtain highly porous and soft intermediates to get fine and non-agglomerated oxide particles. In the conventional Pechini process, however, the addition of polyalcohol-like ethylene glycol which is used to improve the solubility and to aid the esterification of citric acid leads to a severe particle agglomeration during the firing of gel precursors [21,22]. Thus, in order to overcome such a problem, we tried to develop a new synthetic route which utilizes only the chelating ability of the polyfunctional carboxylic acid (citric acid) without using any esterification agents.

As previously pointed out, the chelating ability of citric acid and the complexation between metal ions and citric acid are closely related to the solution pH, and the kinds and concentration of chemical species present in the solution [20]. It is, therefore, required to investigate the chemical species present in an aqueous solution with respect to solution parameters for predicting the optimum preparation condition of amorphous citrate precursors. In the present study, we describe a systematic approach to estimate optimum preparation condition of amorphous citrate precursors based on the theoretical solubility isotherms. Then the crystallization process and particle characteristics of the citrate-derived BAM powder are described in detail along with the preliminary results on the luminescence properties.

2. Experimental section

2.1. Sample preparation

The starting reagents used were high-purity $Ba(NO_3)_3$ (99.98%, Aldrich), $Mg(NO_3)_2 \cdot 6H_2O$ (99.99%, Aldrich), $Al(NO_3)_3 \cdot 9H_2O$ (99.99%, Aldrich), and $Eu(NO_3)_3 \cdot 6H_2O$ (99.99%, Aldrich). A stoichiometric amount of metal nitrates, corresponding to the mole ratio of $Ba_{0.9}Eu_{0.1}MgAl_{10}O_{17}$, were dissolved at first in distilled water, and then a weighed quantity of citric acid ($C_6H_8O_7 \cdot H_2O$) was added to the nitrate solution. The mole ratio of citric acid to the total concentration of metal ions was adjusted to 1.5. After mixing, the solution pH was increased to ca. 7 by dropwise addition of 30% ammonia solution. The water was slowly evaporated off from solution at 80 °C and a transparent metal citrate suspension was formed at first. Further heating, for 1–2 h, at 100–150 °C resulted in dark colored amorphous citrate gels with high viscosity, which were then calcined at 650 °C for 4 h under an air aspiration to remove organic residues. The calcined powder was subsequently heated at 1000 and 1150 °C for 4 h in an ambient atmosphere, and then heated at the temperature range of 1250 and 1350 °C for 2 h under a reducing atmosphere (5% H_2/N_2 mixture gas) for the activation of Eu component.

2.2. Characterization

Thermal reaction of the amorphous citrate precursor was performed under an ambient atmosphere by simultaneous thermogravimetry (TG) and differential thermal analysis (DTA) with a Seiko TG/DTA320 instrument. Crystalline phase evolutions of calcined and sintered BAM powders were examined by powder X-ray diffractometer (MacScience MXP-3) with monochromatic Cu$K\alpha$ radiation ($\lambda = 1.5418$ Å). Elemental analysis of the citrate-derived BAM powder was carried out by inductively coupled plasma (ICP: Perkin-Elmer Optima 3000), for which the sample was fused with lithium metaborate at 900 °C and dissolved in 3% HNO_3 solution. The surface area of samples was measured using the nitrogen gas adsorption multipoint BET method. Field emission electron microscopy (FE-SEM) was carried out with a Hitachi S-4200 electron

microscope, operating at 30 kV. Specimens for electron microscope were coated with Pt–Rh for 180 s under vacuum. X-ray absorption near edge structure (XANES) spectra at Eu L_3-edge were measured on the 3C1 beam line with Si(111) double crystal monochromator at Pohang Accelerator Laboratory (PAL). The data were recorded in steps of 0.03 eV in the fluorescence mode using a silicon solid-state detector at room temperature. The photoluminescence (PL) data were recorded under vacuum UV (VUV) and UV region, using a SPEX Flurolog-2 spectrofluorometer with a deuterium lamp and a Hitachi RF5301 spectrofluorometer with a Xenon flash lamp, respectively. The color coordinates were recorded using a colorimeter (PR-650, Photo Research Co., Ltd.) integrated into the VUV excitation unit.

3. Results and discussion

3.1. Theoretical solubility isotherm

The characteristics of precursor powders prepared by solution routes are highly dependent upon the chemical species present in the solution and the nature of the chemical species is also significantly affected by the solution variables like pH, temperature, concentration and so on. With this point of view, solubility isotherms, which visualize the stability domains of various chemical species as a function of pH versus metal ion concentration (Log[M^{z+}]), may be very helpful for determining the optimum processing conditions. Since the basic principles underlying the construction of solubility isotherms are available in the literature [23], details of numerical calculation are not included here. The possible chemical species and their equilibrium constants considered in this study are summarized in Table 1. Here, we have regarded the pH instead of the concentration of citrates as a master variable to control the equilibrium reactions.

The calculated solubility isotherms for individual metal citrates are superimposed in Fig. 1. For comparison the solubility isotherms for individual metal hydroxide, or carbonate for the case of Ba(II) system, are also overlapped in Fig. 1 with a thin solid line. The open-circled line represents the total concentration of soluble citrates species in equilibrium with each corresponding metal hydroxide or carbonate.

At first, in the $BaCO_3$–citric acid–H_2O system, the possible species, that can be precipitated immediately as solid phases are $Ba(OH)_2$(s) and $BaCO_3$(s). The $Ba(OH)_2$(s) can be precipitated only in a fairly basic region (pH > 13) [24]. Instead of $Ba(OH)_2$(s), therefore, it is more reasonable to consider $BaCO_3$(s) as a stable solid phase under atmospheric environments ($P_{CO_2} = 10^{-3.5}$) [23]. The solubility isotherm of $BaCO_3$(s)

Table 1
Chemical equilibria and the equilibrium constants involved in the $Ba^{2+}/Mg^{2+}/Al^{3+}/Eu^{3+}$–$H_2O$–$CO_3^{2-}$–citric acid system

Equilibrium reaction	Symbol	Log of const.	Ref
$BaCO_3(s) = Ba^{2+} + CO_3^{2-}$	k_{sp}	−8.3	a
$Ba^{2+} + CO_3^{2-} = BaCO_3^0(aq)$	$k_{stab.}$	2.9	a
$Mg(OH)_2(s) = Mg^{2+} + 2OH^-$	k_{sp}	−11.2	b
$Al(OH)_3(s) + 3H^+ = Al^{3+} + 3H_2O$	k_s	8.5	b
$Eu(OH)_3(s) + 3H^+ = Eu^{3+} + 3H_2O$	k_s	17.5	b
$Al^{3+} + H_2O = Al(OH)^{2+} + H^+$	β_1^*	−5	b
$Al^{3+} + 2H_2O = Al(OH)_2^+ + 2H^+$	β_2^*	−9.9	b
$Al^{3+} + 3H_2O = Al(OH)_3^0$ (aq) $+ 3H^+$	β_3^*	−15.6	b
$Al^{3+} + 4H_2O = Al(OH)_4^- + 4H^+$	β_4^*	−23	b
$Eu^{3+} + H_2O = Eu(OH)^{2+} + H^+$	β_1^*	−7.8	c
$Eu^{3+} + 2H_2O = Eu(OH)_2^+ + 2H^+$	β_2^*	−16.6	c
$Eu^{3+} + 3H_2O = Eu(OH)_3^0$ (aq) $+ 3H^+$	β_3^*	−25.6	c
$Eu^{3+} + 4H_2O = Eu(OH)_4^- + 4H^+$	β_4^*	−35.3	c
$C_6H_8O_7 = H^+ + C_6H_7O_7^-$	k_{d1}	−3.1	d
$C_6H_7O_7^- = H^+ + C_6H_6O_7^{2-}$	$k_{d2.}$	−4.8	d
$C_6H_6O_7^{2-} = H^+ + C_6H_5O_7^{3-}$	k_{d3}	−6.4	d
$Ba^{2+} + C_6H_5O_7^{3-} = BaC_6H_5O_7$	$k_{stab.}$	2.6	d
$Ba^{2+} + C_6H_6O_7^{2-} = BaC_6H_6O_7^0$(aq)	$k_{stab.}$	1.8	d
$Ba^{2+} + C_6H_7O_7^- = BaC_6H_7O_7^+$	$k_{stab.}$	0.8	d
$Mg^{2+} + C_6H_5O_7^{3-} = MgC_6H_5O_7^-$	$k_{stab.}$	3.3	d
$Mg^{2+} + C_6H_6O_7^{2-} = MgC_6H_6O_7^0$(aq)	$k_{stab.}$	1.6	d
$Mg^{2+} + C_6H_7O_7^- = MgC_6H_7O_7^+$	$k_{stab.}$	1.1	d
$Al^{3+} + C_6H_5O_7^{3-} = AlC_6H_5O_7^0$(aq)	$k_{stab.}$	20	d
$Al^{3+} + C_6H_6O_7^{2-} = AlC_6H_6O_7^+$	$k_{stab.}$	7	d
$Eu^{3+} + C_6H_5O_7^{3-} = EuC_6H_5O_7^0$(aq)	$k_{stab.}$	7.9	d

[a]Morel, F.F.F. "Principles of Aquatic Chemistry", John Wiley & Sons, New York, 1983.
[b]Baes, C.F. & Mesmer, R.E. "The Hydrolysis of Cations", Wiley & Sons, New York, 1976.
[c]Turner, D.R. Whitfield, M, & Dickson, D.A. *Geochmica et Cosmochimica Acta*, 45, 855, 1981.
[d]Martel, A.E. & Smith, R.M. "Critical Stabilisty Constants", Plenum Press, New York, 1977.

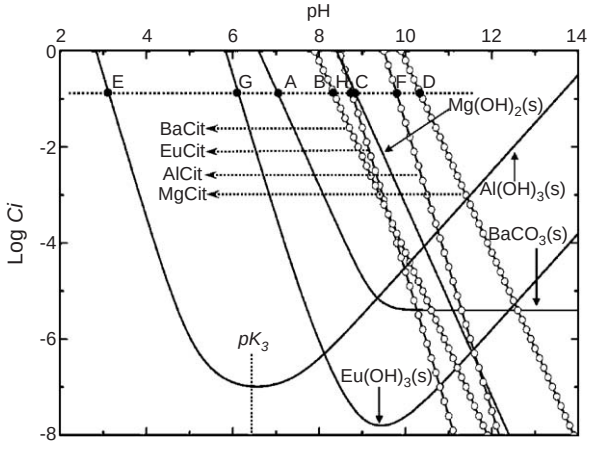

Fig. 1. Solubility isotherms for the $Ba^{2+}/Mg^{2+}/Al^{3+}/Eu^{3+}$–citric acid–$H_2O$ system at 25 °C. The horizontal dotted line denotes the $[M^{z+}] = 0.1\,mol\,dm^{-3}$.

alone shows that the precipitation starts at pH of ca. 7 (point A) when $[Ba^{2+}] = 0.1\,mol\,dm^{-3}$ (dotted line). However, when citric acid is present as a chelating

agent, the solubility of $BaCO_3$(s) increases due to the formation of soluble Ba–citrate complexes such as $Ba(C_6H_7O_7)^+$, $Ba(C_6H_6O_7)^0$ and $Ba(C_6H_5O_7)^-$. The total concentration of soluble Ba–citrate complexes ($= [Ba(C_6H_7O_7)^+] + [Ba(C_6H_6O_7)^0] + [Ba(C_6H_5O_7)^-]$) at equilibrium with a solid $BaCO_3$(s) is also shown in Fig. 1. When the citric acid is present in Ba^{2+}-containing aqueous solution, Ba^{2+} preferentially forms complexes with citric acid, so that the precipitation of $BaCO_3$(s) does not occur until the pH reaches ca. 8.5 (point B). In the Mg(II)–citric acid–H_2O system, the precipitation of $Mg(OH)_2$(s) occurred at the basic pH domain (pH > 9, point C) when the citric acid was absent, while the precipitation of solid $Mg(OH)_2$(s) was strongly retarded (pH > 10.5, point D) due to the formation of soluble Mg citrates like $Mg(C_6H_7O_7)^+$, $Mg(C_6H_6O_7)^0$ and $Mg(C_6H_5O_7)^-$ in the presence of citric acid. In other words, the pure and stable magnesium citrate can be formed below the solution pH of 10.5. The formation of $Al(OH)_3$(s) in the absence of citric acid begins at a considerably lower pH of about 3 (point E) because of the strong hydrolysis tendency of Al^{3+} ion. However, the $Al(OH)_3$(s) precipitation is strongly suppressed when citric acid exists as a complexing agent and, therefore, the hydroxide precipitation is only possible above pH = 9.7 (point F). Aluminum citrates such as $Al(C_6H_6O_7)^+$ and $Al(C_6H_5O_7)^0$ exist as predominant species instead of hydroxyl complexes. Similarly, the precipitation of $Eu(OH)_3$ can occur at pH of ca. 6 when $[Eu^{3+}] = 0.1\,mol\,dm^{-3}$ (point G), which shifts to a basic pH domain (pH = 8.7, point H) due to the formation of europium citrate complexes. Finally, by taking the dissociation of citric acid into account, it is desirable to work at pH > pK_3 (6.44, Table 1) to ensure the complete dissociation of citric acid. Also, in order to obtain pure and stable citrate complexes of Ba^{2+}, Mg^{2+}, Al^{3+}, and Eu^{3+} simultaneously, the solution pH should be maintained at 6 < pH < 8. Thus, it can be concluded that the optimum condition is pH of ca. 7 for the formation of pure and stable metal citrate complexes without any secondary phases, such as hydroxide and carbonate.

3.2. Thermal analysis

The thermal decomposition of citrate precursor of BAM is shown in Fig. 2. Below 200 °C there is a gradual weight loss in TG and an endothermic peak in DTA due to the dehydration of free water. Between 200 and 650 °C, an exothermic reaction takes place with a large weight loss, which corresponds to the oxidative decomposition of residual organics (citrate and its thermal derivatives). It can be therefore said that most of the organics are burnt off below 650 °C. An additional endothermic reaction occurs at around 980 °C with a significant weight loss in TG, which can be ascribed to

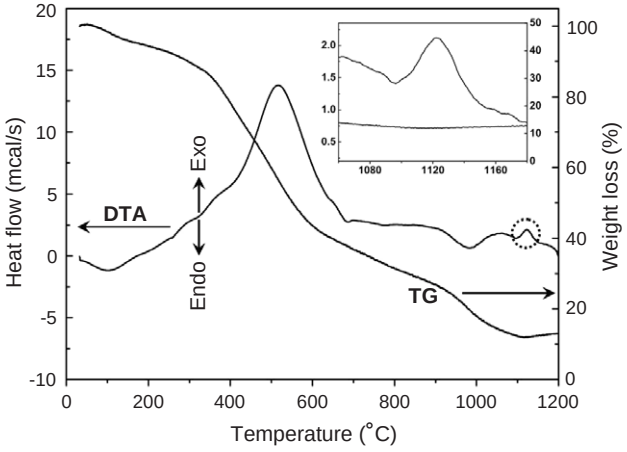

Fig. 2. TG and DTA curves for the metal citrate precursor (heating rate = 10 °C/min.).

the decomposition of intermediate metal carbonates formed during the firing of metal citrate precursor. Finally, a weak but clearly discernable exothermic peak was observed at 1120 °C. Since there is no distinct weight change at this temperature region (the inset in Fig. 2), this exothermic reaction can be assigned to the crystallization of BAM phase from amorphous material.

3.3. Elemental analysis

To evaluate the cation stoichiometry of the citrate-derived BAM powder, the sample heated at 1250 °C in a reducing atmosphere was analyzed by ICP method. The averaged chemical composition of BAM powder was determined to be $Ba_{0.903}Eu_{0.089}Mg_{1.006}Al_{10.0}O_{17.043}$ from the three-time measurements. Such a result confirms that the citrate sol–gel process is quite effective for producing stoichiometric BAM powders.

3.4. Powder X-ray diffraction analysis

In order to understand the crystallization behavior of BAM from amorphous citrate precursor, temperature-resolved X-ray diffraction patterns were measured as represented in Fig. 3. The powders obtained after firing the metal citrate precursor at 650 °C (a) show characteristics of the amorphous phase. The amorphous character of the precursor is resisted up to 1000 °C, (b) even though minor intermediate phases like $BaAl_2O_4$ and δ-Al_2O_3 appear. When the temperature increases up to 1150 °C (c), patterns of BAM appear without any other impurities, which is in good agreement with the expectation from the TG analysis that a rapid crystallization of amorphous materials could occur at around 1120 °C. Though the crystallization of BAM is not still enough, this crystallization temperature is lower than about 400 °C in comparison with that of the conventional solid-state reaction without flux [5]. It should be

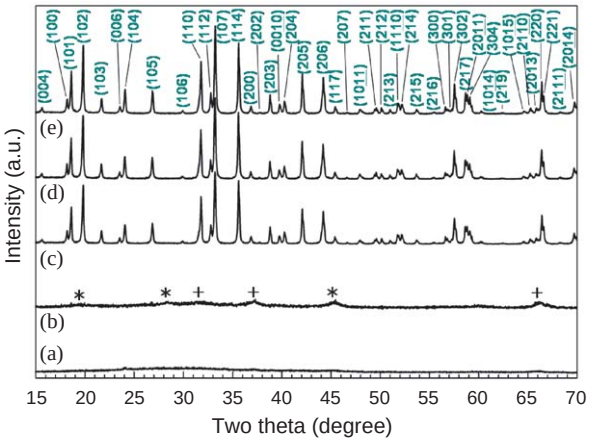

Fig. 3. Powder X-ray diffraction patterns of the samples heated at 650 °C (a), 1000 °C (b), 1150 °C (c) under an ambient atmosphere. (d) and (e) correspond to the samples heated at 1250 and 1350 °C under a reducing atmosphere, respectively. Symbol "∗" and "+" in (b) denote $BaAl_2O_4$ and δ-Al_2O_3, respectively.

also noted that all of the diffraction patterns are perfectly indexed as the crystalline BAM phase, whereas some patterns with low intensity could not be indexed or observed in the most previous works using the conventional solid state or sol–gel methods. In the metal citrate sol–gel process, the high degree of mixing of each metal component on an atomic level in the precursor stage is primarily responsible for the significant lowering of crystallization temperature of barium hexaaluminate. In addition, the large reactive surface area ($S_{BET} = 88\,m^2/g$) of the precursor powders developed while firing the metal citrate at 650 °C would also facilitate the rapid crystallization. When the sample that was crystallized at 1150 °C was subsequently sintered at 1250 or 1350 °C under a reducing atmosphere, there was no appreciable change in the diffraction patterns except for the increased intensities (d and e). This implies that BAM crystallizes completely at around 1250 °C and a reducing atmosphere mainly contributes a simple reduction of Eu^{3+} to Eu^{2+}. According to Kimura et al. [25] and Smets et al. [26], the splittings in (107) and (00*l*) reflections, respectively, are diagnostic indicators of the phase multiplicity due to non-stoichiometry of metal cations in BAM structure. In the citrate-derived BAM powders, however, no appreciable splitting is revealed in any one of these reflections even under slow scanning mode for high resolution, which is indicative of the high structural homogeneity of the citrate-derived BAM powders.

3.5. X-ray absorption spectroscopy

Luminescent characteristics of Eu-doped BAM strongly depend on the crystal structure, phase purity, and the amount of Eu^{2+} ions [2,27]. Though the crystal structure and phase purity could be checked by powder X-ray diffraction as mentioned above, the oxidation states and local environments of the doped europium ions are still in question. Fortunately, it is well known that the L_3 absorption edge of rare earth element exhibits the sharp and strong X-ray absorption peak at its higher energy side [28,29]. This strong absorption peak corresponds to an electron transition from $2p_{3/2}$ core level to the lowest unoccupied $5d6s$ state, and its position and shape are very sensitive to the valence state and the chemical environment of the absorbing atom. For this reason, we applied XANES spectroscopy to elucidate the valence state and the chemical environment of the europium ions upon the preparation condition of samples. Fig. 4 shows the XANES spectra at Eu L_3-edge for the samples prepared at various temperatures, in which the spectrum of Eu_2O_3 is included as a reference. The XANES spectrum for the sample calcined at 1000 °C in an ambient atmosphere exhibits two strong absorption peaks centered at 6972 and 6979.5 eV. Considering the energy difference of 7.5 eV [30,31] and the position of absorption peak of Eu_2O_3 used as a reference of trivalent europium ion, each peak at 6972 and 6979.5 eV corresponds to the divalent and trivalent oxidation state of europium, respectively. XANES spectrum for the sample treated at 1150 °C shows the conspicuous reduction of europium ions even in non-reducing atmosphere, which suggests that the crystallization of BAM structure allows the covalency of the Eu–O bond to increase and induces the conversion from Eu^{3+} to Eu^{2+}. In a reducing atmosphere, the peak at higher energy corresponding to trivalent europium gradually decreased upon the increasing temperature and finally disappeared at 1350 °C, indicating the existence of only divalent europium. XANES spectrum also contains the local structural information around the

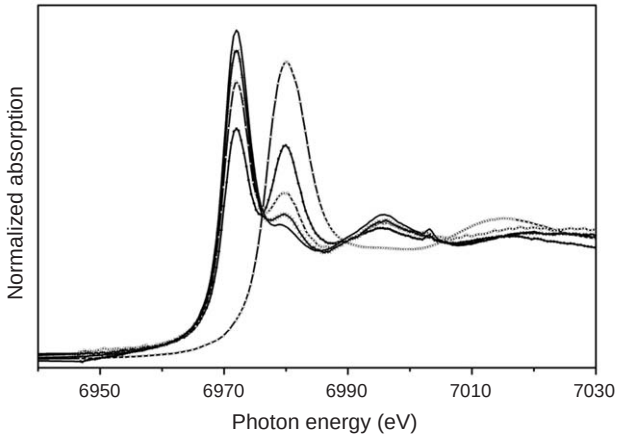

Fig. 4. Eu L_3-edge XANES spectra for the samples at 1000 °C (line with solid circle), 1150 °C (line with empty circle) under an ambient atmosphere, and 1250 (line with cross), 1350 °C (solid line) under a reducing atmosphere. Eu_2O_3 (line with triangle) was used as a reference.

absorbing atom [32]. Spectral oscillations in the region (above about 6990 eV) above the absorption edge result from the multiple scatterings of the photoelectron between the central absorbing atom and neighboring atoms. The difference between the spectral oscillations of Eu_2O_3 and Eu-doped BAM samples in this region as clearly shown in Fig. 4 is due to the local structural difference around europium. It is worth noting that the sample calcined at 1000 °C in an ambient atmosphere is crystallographically amorphous but the local structure around europium ions are almost the same with crystalline samples.

3.6. Particle morphology

Fig. 5 shows the SEM photographs of the citrate-derived BAM particles thermally treated at the given temperatures and atmospheres. The powders obtained at 1000 °C are mainly composed of quite spherical particles with the diameter of ~25 nm (a). The bulky organic residues present in metal citrate precursor strongly suppress the particle agglomeration during firing and sintering processes, which is favorable to the formation of nanometer size particles. It should be noted here that the exclusion of esterification agent (ethylene glycol) through optimizing the metal-citrate complexation by a simple pH control plays a crucial role in preparing the monodispersive nanoparticles. The reduction of organic residues in the gel precursor on the basis of theoretical consideration of solubility isotherms leads to minimizing of the surplus combustion heat during pyrolysis, causing a severe particle agglomeration, which enables us to prepare non-agglomerated nanoparticles

After further increase of the heating temperature to 1150 °C (b), overall spherical morphology and particle size remain almost constant without any significant particle agglomeration. As mentioned from the TG and XRD analyses, the crystallization of amorphous material into crystalline BAM occurred at this temperature. Nevertheless, particle morphology is not plate-like and thus characteristic to BAM particle but spherical. Further raising the temperature to 1250 °C (c) and 1350 °C (d), the agglomeration of primary nanoparticles is slightly enhanced and the morphology of the secondary particles turns from spherical to rounded-cube, or in part, columnar shapes, which can be considered as a result of the crystal growth addressed by the crystallographic direction of hexaaluminate. It is worthy to note here that the primary spherical nanoparticles remain almost unchanged. The primary particle size is found to be 20–30 nm, which shows good agreement with the value estimated from X-ray line broadening.

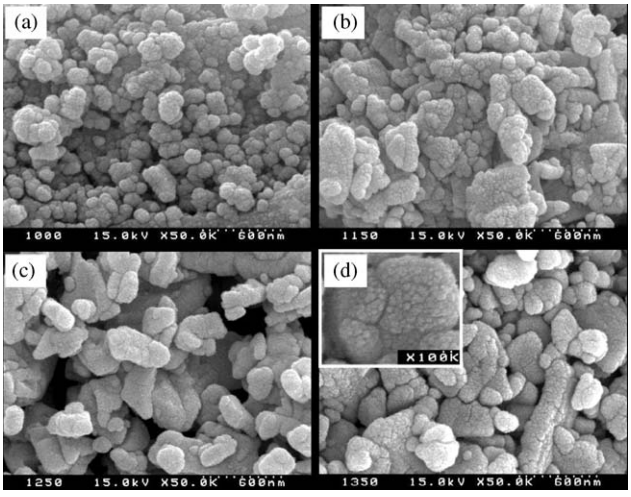

Fig. 5. Scanning electron micrographs for the samples at 1000 °C (a), 1150 °C (b) under an ambient atmosphere, and 1250 °C (c), 1350 °C (d) under a reducing atmosphere.

3.7. Photoluminescence spectroscopy

The excitation spectra of $BaMgAl_{10}O_{17}$:Eu samples prepared at various post-treatment temperatures were measured by monitoring the blue emission at 450 nm, and are compared with that of a commercial BAM phosphor (Nichia Co., Ltd.) in Fig. 6. It is clearly seen that the luminous intensities of the present samples are lower that that of a commercial phosphor, especially in the VUV region. Fig. 7 shows that the emission spectra excited at 147 nm (a) and 254 nm (b), respectively. As expected from the excitation spectra of Fig. 6, the emission intensities of the present samples increased with the post-treatment temperature under both the excitation wavelengths. The highest emission intensity was observed with the sample post-treated at 1350 °C under UV (254 nm) excitation, but under VUV (147 nm) excitation the commercial phosphor exhibited the highest emission intensity. This fact can be explained by considering the difference of a penetration depth of the irradiated beam of VUV (147 nm) or UV (254 nm). As the excitation wavelength becomes short, the penetration depth is decreased and the excitation volume from which PL is observed moves closer to the surface [33]. Since the particle surface can substantially act as a defect or a source of non-radiative recombination routes, the larger surface area due to the fine phosphor particle will result in lower luminescent efficiency under VUV irradiation than under UV irradiation. In addition, the local structure change of the host and the activator ion should be considered in order to understand the PL intensity and the color coordinates. Because the atomic arrangement on the particle surface is different from that of the bulk lattice, the fine phosphor particle with a large surface area will be more influenced by VUV irradiation than by UV irradiation. In fact, the emission peak shift accompanying the

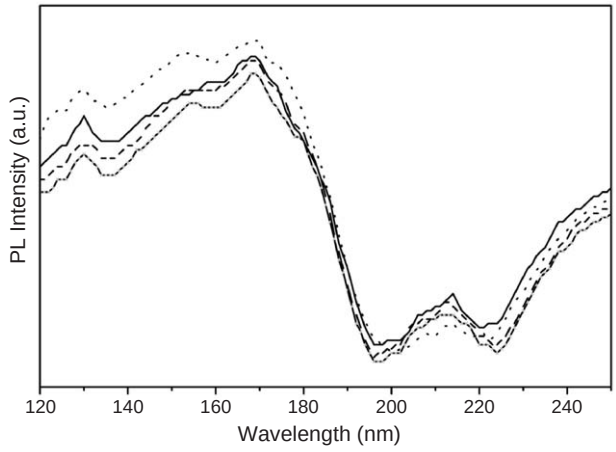

Fig. 6. Excitation spectra of phosphors in VUV region for the samples at 1150 °C (line with cross), 1250 °C (dashed line), and 1350 °C (solid line) with commercial BAM (dotted line).

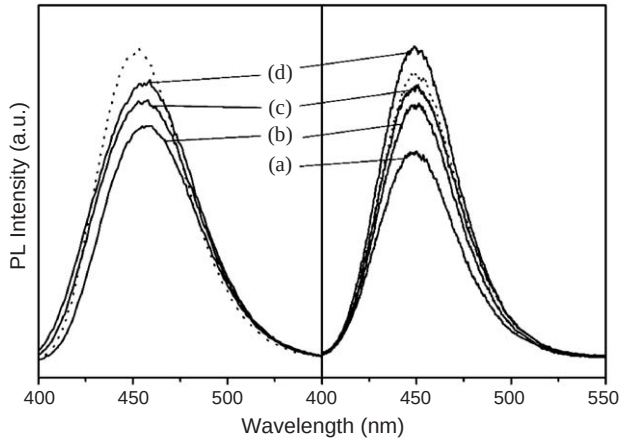

Fig. 7. Emission spectra under the excitation of 147 nm (left) and 254 nm (right) for the samples at 1000 °C (a), 1150 °C (b), 1250 °C (c), and 1350 °C (d) with commercial BAM (dotted line).

intensity change is observed in Fig. 7, which might be due to the local structure changes of BAM and Eu^{2+} ion on the particle surface. All emission spectra under UV excitation of Fig. 7(right) exhibit the maximum intensity at 450 nm, while in Fig. 7(left) the maximum emission intensity of the present samples is shifted to longer wavelength in comparison with that (450 nm) of the commercial phosphor with an average particle size of about 7 μm. The CIE color coordinates for the present samples under VUV excitation exhibit lower x and higher y coordinates than those of the commercial phosphor as shown in Table 2. As the post-treatment temperature increases from 1150 to 1350 °C, the crystal growth occurs and the influence of surface decreases, resulting in the color coordinates of the present samples approaching those of the commercial phosphor. It should be also noted that under VUV excitation the sample heat-treated at 1350 °C exhibits the higher

Table 2
Luminous properties under the 147 nm excitation according to the synthetic temperatures

Samples	Color coordinates		Relative luminance (%)
	x	y	
1150 °C	0.136	0.112	81
1250 °C	0.139	0.097	93
1350 °C	0.141	0.085	105
Commercial BAM	0.145	0.067	100

luminance (about 5%) in comparison with that of the commercial phosphor as shown in Table 2, which might be also due to the color shift. Consequently, UV excitation well reflects the luminescent properties of the bulk particle, while under VUV excitation the surface character would have a great influence on the luminescent properties, especially for the fine phosphor particle. However, we have ruled out the possibility of the enhanced luminescence by the smaller phosphor particle. As the penetration depth of the excited beam becomes short, the ratio of the dead volume in phosphor particle, into which the excited beam cannot reach, would increase. That is, though the large surface itself of a fine particle is detrimental to the luminescent characteristics, the reduction of the dead volume ratio would be profitable to the luminescence, especially under the irradiation of the short wavelength like VUV. Therefore, the optimum particle size as well as the crystallographic condition should be considered for the synthesis of a phosphor with the best luminescent properties.

4. Conclusions

A novel low-temperature route to homogeneous and stoichiometric BAM phosphor powder using metal citrate complex was proposed on the basis of theoretical consideration of solubility isotherms. From the calculation of solubility isotherms for metal ions–citric acid–H_2O systems at 25 °C, the optimum pH condition for preparing pure and stable metal citrate complexes was determined to be pH = 7. Well-crystallized and submicrometer-sized BAM particles could be obtained by thermal decomposition of the optimally prepared citrate precursor at a temperature as low as 1150 °C. High degree of mixing of each metal component on an atomic level and the large reactive surface area ($S_{BET} = 88\,m^2/g$) of the precursory powders play an important role in the significant lowering of crystallization temperature of barium hexaaluminate. The citrate sol–gel process has great potential for producing high efficient blue-emitting BAM phosphor at lower processing temperature under

the optimization of variables such as doping level of Eu, processing conditions, and particle size and morphology.

Acknowledgment

The authors gratefully acknowledge the financial support of the Korea Research Foundation (KRF-2003-070-C00029).

References

[1] D. Ravichandran, S.T. Johnson, S. Erdei, R. Roy, W.B. White, Displays 19 (1999) 197.
[2] K.-B. Kim, Y.-I. Kim, H.-G. Chun, T.-Y. Cho, J.-S. Jung, J.-G. Kang, Chem. Mater. 14 (2002) 5045.
[3] G. Blasse, J. Alloys Compd. 192 (1993) 17.
[4] S. Ekambaram, K.C. Patil, J. Alloys Compd. 248 (1997) 7.
[5] S. Oshio, K. Kitamura, T. Shigeta, S. Horii, T. Matsuoka, S. Tanaka, H. Kobayashi, J. Electrochem. Soc. 146 (1999) 392.
[6] B.M.J. Smets, J.G. Verlijsdonk, Mater. Res. Bull. 21 (1987) 1305.
[7] C.R. Ronda, J. Lumin. 72–74 (1997) 49.
[8] T. Jüstel. H. Bechtel, D.U. Wiechert, Sixth International Conference on Sci. Tech. Display Phosphors, San Diego, CA, 2000, p. 17.
[9] N. Iyi, Z. Inoue, S. Takekawa, S. Kimura, J. Solid State Chem. 52 (1984) 66.
[10] S. Oshio, T. Matsuoka, S. Tanaka, H. Kobayashi, J. Electrochem. Soc. 145 (1998) 3898.
[11] J.M.P.J. Verstegen, J. Electrochem. Soc. 121 (1974) 1623.
[12] A.T.N. Stevels, A.D.M. Schrama-de Pauw, J. Electrochem. Soc. 123 (1976) 691.
[13] B. Smets, J. Rutten, G. Hoeks, J. Verlijsdonk, J. Electrochem. Soc. 136 (1989) 2119.
[14] D. Ravichandran, R. Roy, W.B. White, S. Erdei, J. Mater. Res. 12 (1997) 819.
[15] Y.C. Kang, S.B. Park, J. Electrochem. Soc. 147 (1997) 799.
[16] Y.C. Kang, S.B. Park, I.W. Lenggoro, K. Okuyama, J. Electrochem. Soc. 146 (1999) 2744.
[17] B.S. Jeon, G.Y. Hong, Y.K. Yoo, J.S. Yoo, J. Electrochem. Soc. 148 (2001) H128.
[18] M. P. Pechini, US Patent No. 3,330, 697, July 1967.
[19] J. Zhang, Z. Zhang, Z. Tang, Z. Zheng, Y. Lin, Powder Technol. 126 (2002) 161.
[20] J.-H. Choy, Y.-S. Han, S.-H. Hwang, S.-H. Byeon, G. Demazeau, J. Am. Ceram. Soc. 81 (1998) 3197.
[21] L.W. Tai, P.A. Lessing, J. Mater. Res. 7 (1992) 502.
[22] L.W. Tai, P.A. Lessing, J. Mater. Res. 7 (1992) 511.
[23] T.M.M. Morel, Principles of Aquatic Chemistry, Wiley, New York, 1983.
[24] J.-H. Choy, Y.-S. Han, J.-T. Kim, Y.-H. Kim, J. Mater. Chem. 5 (1995) 57.
[25] S. Kimura, E. Bannai, I. Shindo, Mater. Res. Bull. 17 (1982) 209.
[26] B. Smets, J. Rutten, J. Hoeks, J.G. Verlijsdonk, J. Electrochem. Soc. 136 (1989) 2119.
[27] T.R.N. Kutty, M. Nayak, Mater. Chem. Phys. 65 (2000) 158.
[28] F.W. Lytle, G. Van der Laan, E.M. Larson, C.E. Violet, J. Wong, Phys. Rev. B 41 (1990) 8955.
[29] J.-H. Choy, D.-K. Kim, S.-H. Hwang, G. Demazeau, D.-Y. Jung, J. Am. Chem. Soc. 117 (1995) 8557.
[30] F. Liu, M. Zhu, T. Liu, Mater. Sci. Eng. B 81 (2001) 179.
[31] H. Liang, H. He, Q. Zeng, S. Wang, Q. Su, Y. Tao, T. Hu, W. Wang, T. Lie, J. Zhang, X. Hou, J. Electron Spectrosc. Relat. Phenom. 124 (2002) 67.
[32] D.-K. Kim, S.-H. Choi, Y.-S. Han, H. Yun, J. Synchrotron Radiat. 8 (2001) 734.
[33] B. Moine, G. Bizarri, Mater. Sci. Eng. B 105 (2003) 2.